PROCEEDINGS, 49th Workshop on Geothermal Reservoir Engineering
Stanford University, Stanford, California, February 12-14, 2024
SGP-TR-227

Dieng Reservoir Numerical Model: A Robust Update

Marchel C. Supijo, Ichwan A. Elfajrie, Zahratul Kamila, Elfina, Reza Jamil Fajri, Julia A. Alibazah, Aditya Y. Kencana, M. Istiawan Nurpratama, and Ali Ashat

PT. Geo Dipa Energi (Persero), Aldevco Octagon 6th Floor, Jl. Hj. Tutty Alawiyah No. 75, Pejaten Barat, Pancoran, Jakarta Selatan, DKI Jakarta, Indonesia

marchel@geodipa.co.id

Keywords: Dieng geothermal field, numerical model

ABSTRACT

PT Geo Dipa Energi (Persero) started developing Dieng Geothermal Field in 2002 with an installed plant capacity of 60 MWe. Dieng numerical models were developed in 2006, 2013, and 2019. The latest Dieng numerical model was built in 2019 as the basis of the feasibility study for Dieng 2 development. With additional Dieng 2 wells data, comprehensive assessment of production and injection data of Dieng 1, and deep analysis of PT shut-in data, the updated numerical model is more robust than the previous model developed in 2019. This model considers two reservoir compartments, i.e., Sileri and Sikidang. The natural state and history matching for 20 years of Dieng 1 production indicated the extension (horizontally and vertically) of the steam cap distribution in the Sileri area.

1. INTRODUCTION

Dieng numerical model has been developed by various consultant entities, i.e., West JEC (2007), ELC (2013), and through a collaborative effort involving GDE, ADB, and ITB in 2019 (Ashat et al., 2019). This paper will implement an update to the model established in 2019, referred to from the conceptual model enhancements. The grid block size is readjusted with greater granularity, accompanied by the dimensions of the area of interest. At the same time, the dynamics of reservoir volume derived from findings from the Dieng Unit 2 drilling endeavor are considered. PT Geo Dipa Energi (Persero) conducted this reservoir numerical simulation internally using PetraSim® (a TOUGH2 user interface).

2. NATURAL STATE

2.1 Computer Model

The delineation of the reservoir model used refers to the proven area boundaries (Figure 1). By considering the condition of the main structure of the Dieng geothermal field with the predominant NW-SE trend, the computer model is rotated by 317 degrees to align horizontally with the cross-section of the conceptual model.

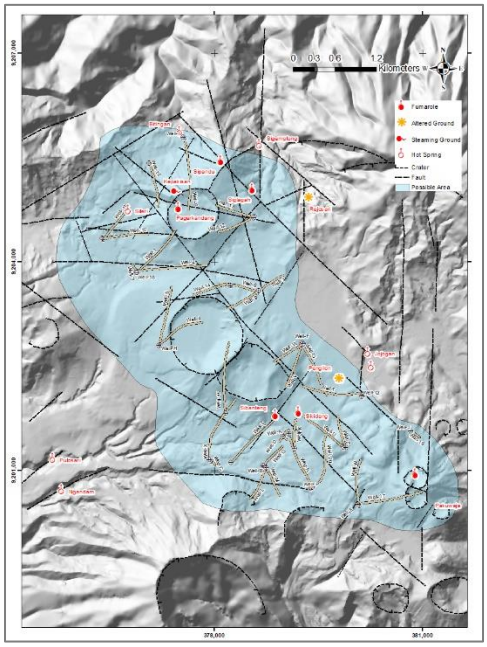

Figure 1: Reservoir boundary of Dieng geothermal field

Rotating the model aims to facilitate a comprehensive understanding of the heat and mass flow within the reservoir (Supijo et al., 2019). The total area the model covers is approximately 14.1 km x 12.9 km (183 km^2), including the surrounding rock formations (Figure 2). The extensive coverage of the model ensures a substantial distance between the reservoir and its boundaries, thereby minimizing the potential impact of boundary conditions on model performance. The constructed model faithfully represents the conditions prevailing in the Dieng geothermal field, with layers tailored to match the actual topographic characteristics of the area closely.

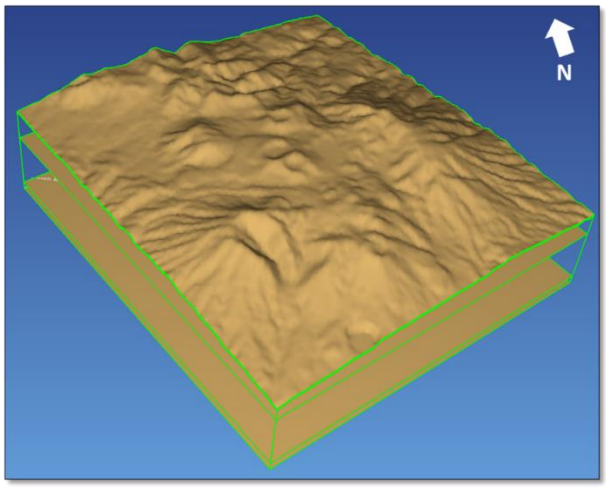

Figure 2: Top boundary computer model based on topographic conditions of the Dieng geothermal field

2.1.1 Gridding & Layering

The models exhibit vertical thicknesses ranging from 2,715 meters to 5,149 meters. This variance in thickness arises from the disparity between the lowest and highest topographical elevations, ranging from 715 meters above sea level (masl) to 3,149 masl, with the lower boundary of the model situated at a depth of -2000 masl. The model is divided into six main layers, i.e., atmosphere, groundwater, cap rock, reservoir 1, reservoir 2, and basement (Table 1). The atmosphere and groundwater layers maintain a uniform thickness of 50 meters. The cap rock layer is subdivided into four sub-layers, each with variable thickness determined by topographic conditions. The reservoir layer is bifurcated into two primary layers: reservoir 1, which is thinner at 150 meters and comprises ten sub-layers extending to a depth of -750 masl, and reservoir 2, relatively thicker at 250 meters with four sub-layers reaching a depth of -1,750 masl. The partitioning of the two primary reservoir layers aligns with the availability of the deepest temperature measurements in the WELL-15 well, recorded explicitly at an elevation of -785 masl. The basement segment spans a thickness of 250 meters, ranging from -1,750 masl to -2,000 masl. In total, the model comprises 21 horizontal layers.

Table 1: Model layer

Layer	Ketebalan	Ukuran Cell (meter)	Cell
Atmosphere (ATM)	50 m above topography	50	1
Groundwater (GW)	50 m below topography	50	1
Caprock (CAPR)	Groundwater up to 750 mdpl	Varies with topographic	4
Reservoir 1 (RES1)	750 masl up to -750 masl	150	10
Reservoir 2 (RES2)	-750 masl up to -1750 masl	250	4
Basement (BASE)	-1750 masl up to -2000 masl	250	1
		Total	**21**

Figure 3 illustrates the grid structure of the model. The type of grid used is rectangular. The highlighted region within the yellow dotted box denotes the area of interest corresponding to the reservoir zone. Specifically, the reservoir area is delineated as 50 m x 50 m, 200 m x 50 m, and 200 m x 200 m. The smallest grid block size (50 m x 50 m) is in the wellpad 29. In comparison, the 200 m x 50 m dimension is allocated to the upflow zone within the Dieng geothermal field, specifically the Sileri, Merdada, and Sikidang areas. Each layer has 2,214 grid blocks, resulting in 46,494 grid blocks across the 21 layers.

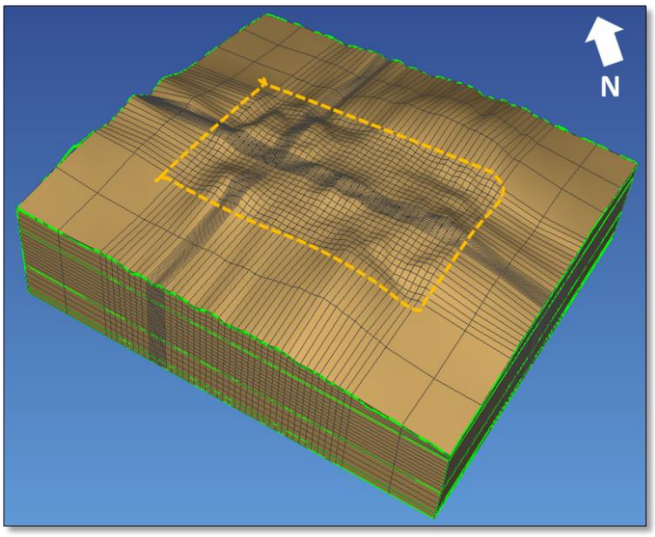

Figure 3: Model gridding

2.1.2 Internal Boundary

Internal boundaries represent the models' structures based on geoscience investigations and well data analysis (Pratama et al., 2020). These boundaries facilitate the delineation of structural elements, including both permeable and impermeable materials. Structural material properties are defined exclusively on internal boundaries within the reservoir area, which governs the Dieng geothermal system, rather than across all internal boundaries. Figure 4 shows the internal boundaries integrated into the model. A total of 20 structures have been incorporated. These structures have been selected based on a fault ranking assessment conducted by the geoscience team, ensuring high confidence in their inclusion.

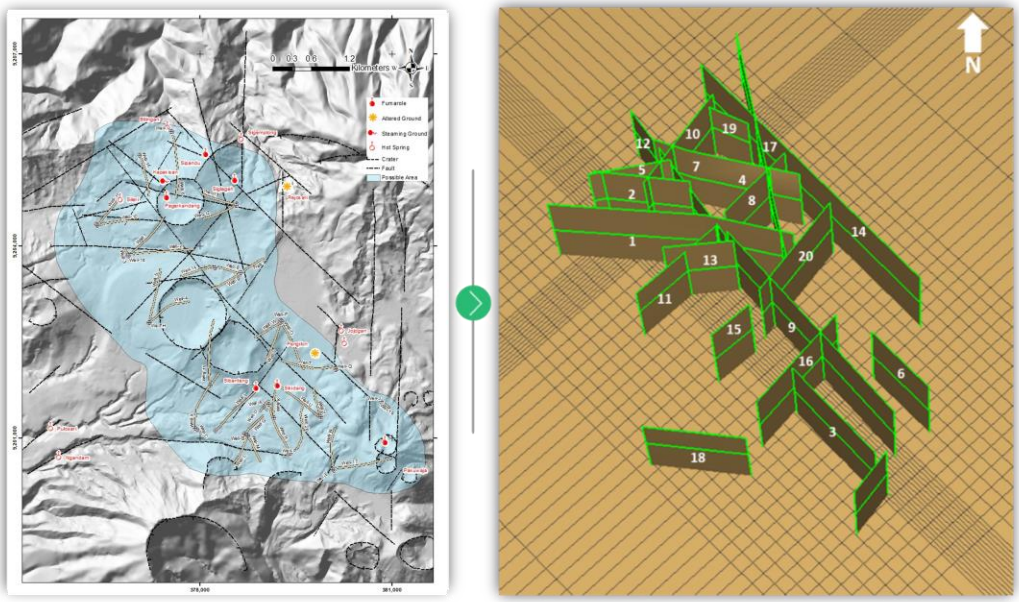

Figure 4: The structure is delineated within the model as an internal boundary

2.1.3 General Parameter

The simulation of the Dieng geothermal field reservoir using TOUGH2 V.2.0. software, utilizing Equation of State (EOS) 1 for water and water with tracer. This EOS accounts for fluid properties, encompassing water and steam, while excluding consideration of Non-Condensable Gas (NCG) and dissolving solid conditions within this simulation. The transient phenomena in fracture-dominated reservoir systems are modeled using the dual porosity model with the MINC (multiple interacting continua) approach (Pruess and Narasimhan,1985). This model uses two interacting continua, as illustrated in Figure 5, where each grid block comprises a matrix and fracture, each with its own porosity and permeability attributes. Within the MINC approach, two parameters notably influence the variations observed in the numerical model: fracture volume fraction and fracture spacing. The fracture volume fraction inputted into the model is set at 5%. This determination arises from the outcomes of iterations conducted during the natural state and history matching

stages. It has been observed that the model exhibits a more pronounced pressure decline, attributable to a reduced mass within the rock if the fracture volume fraction falls below 5%. Thus, a fracture volume of 5% is deemed the most conservative value for the Dieng geothermal field. The fracture spacing is also established at 50 meters, corresponding to the condition of the smallest grid block size in the model.

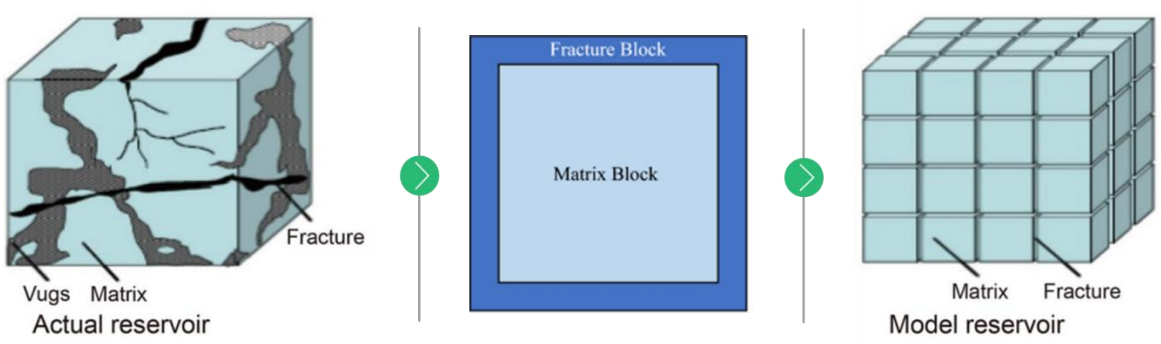

Figure 5: Representation of the actual fracture-dominated reservoir in the dual porosity model (Warren and Root, 1963)

2.1.4 Pressure and Temperature QC

A total of 5 gradient holes (TCH) and 47 wells have been drilled within the Dieng field. Pertamina conducted 27 wells during the period from 1977 to 1993, while California Energy drilled 20 wells between 1995 and 1998. Figure 6 shows the static temperature data quality distribution for the Sileri and Sikidang areas, respectively. In general, wells with good data quality (colored green) will be used as a reference for validating the numerical model at the natural state stage. However, several wells in partially stable condition in the Sileri area are also being considered at this stage. Thus, the total wells included in the PT matching numerical model for the Dieng geothermal field are 25 wells, consisting of 18 wells in the Sileri area and seven wells in the Sikidang area.

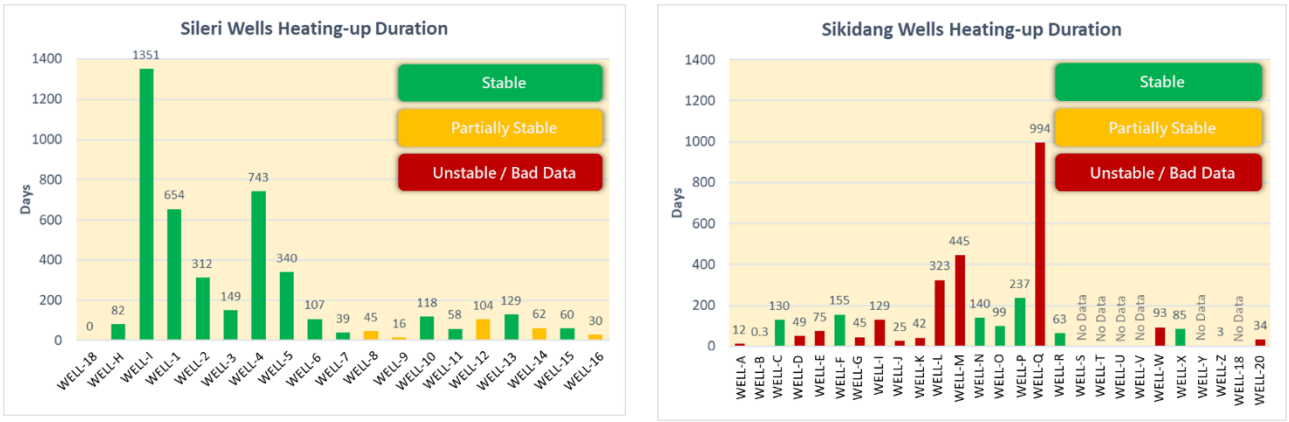

Figure 6: Static temperature data quality (a) Sileri wells; (b) Sikidang wells

As the well heats up, a concurrent change in fluid density occurs. However, the pressure in the feed zone area will remain at the reservoir pressure condition. The water column in the well will rise when this process occurs, resulting in the shallow water column depth and the pressure profile intersecting in the feed zone area. This intersection is a pivot point to determine the pressure profile per depth. The data used is pressure logging data for wells in shut-in conditions. The assessment of pressure distribution in the Dieng geothermal field is bifurcated into two segments: evaluating pressure distribution in wells located within the Sileri and Sikidang areas. This is based on geoscience analysis, which suggests distinct reservoir conditions within the Dieng geothermal field. The outcomes of this evaluation will serve as a benchmark for validating pressure under natural state conditions.

The compilation of pressure distribution results reveals that the Sileri area exhibits higher pressure compared to the Sikidang area. Furthermore, Figure 7 illustrates distinct pressure gradients in these two areas. This observation strongly suggests the presence of different heat sources in these regions, which directly influence pressure support for each reservoir area. However, it is essential to acknowledge that the pressure distribution in the Sikidang area remains uncertain due to poor data quality, with the regression pivot quantity derived from only four wells.

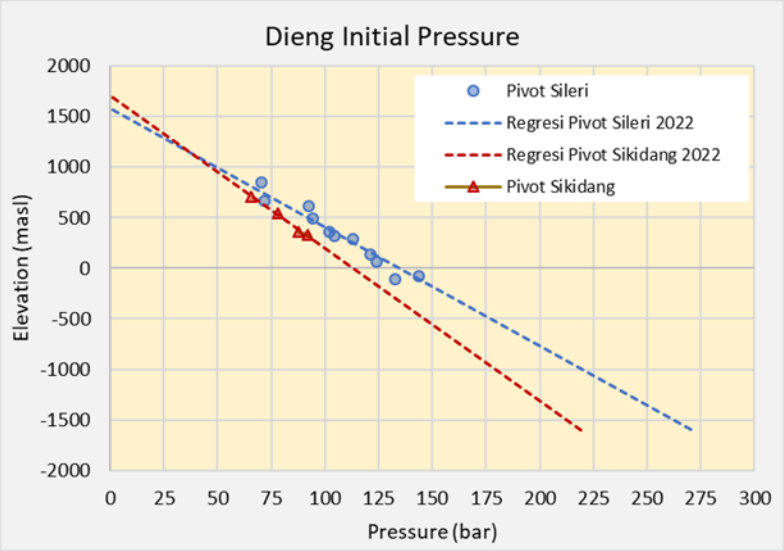

Figure 7: The compilation of the pressure distribution within the Dieng geothermal field

2.1.5 Conceptual Model

The cap rock exhibits thinning beneath Pangonan Crater, Merdada Crater, and Pangonan-Sikidang Crater while it thickens towards the system's periphery. The determination of cap rock thickness is substantiated by temperature gradient data, which identifies conductive areas.

The geochemical data from wells indicates notable differences in fluid characteristics between the Sileri and Sikidang areas. Generally, the fluid character in the Sileri area is neutral, albeit with a potential magmatic fluid influx in the Merdada Crater vicinity. Reservoir rocks in the Sileri area encompass the Gajahmungkur unit and the Andesite Complex unit, exhibiting temperatures ranging from approximately 283°C to 338°C, with a Top of Reservoir (TOR) elevation spanning 400 to 800 masl. Fluid from the Sileri area reservoir is characterized by low Non-Condensable Gas (NCG) content (< 1wt%) and is classified as mature chloride brine, featuring high chloride content ranging from 9,600 to 19,000 mg/kg. Given the fluid characteristics and high reservoir temperatures in the Sileri area, there is potential for scaling in the wellbore, particularly in silica and metal sulfide. Metal sulfide scaling has been observed in all production wells in the Sileri area. In contrast, silica scaling has been identified in only a few production wells, possibly due to operational practices that maintain them above the Sulfide Saturation Index (SSI).

In contrast to the Sileri area, the reservoir in the Sikidang area exhibits a more acidic fluid character attributed to the predominant influence of magmatic fluid. However, the spatial distribution of this acidic influence has yet to be determined. Reservoir rocks in the Sikidang area comprise the Old Dieng Lava unit and the Andesite Complex unit, with reservoir temperatures ranging from approximately 250°C to 324°C and a TOR elevation spanning 700 to 800 masl. Fluid from the Sikidang area reservoir is characterized by high chloride (Cl), boron (B), arsenic (As), and Non-Condensable Gas (NCG) contents (2 – 17 wt%), indicating characteristics resulting from the mixing of mature chloride brine and volcanic sulfate water. Analysis of fluid characteristics in Pakuwaja utilized data from two wells, namely WELL-17 and WELL-E, revealing bicarbonate water types. However, the brine data from these two wells includes immature water, precluding further analysis. Gas data from the WELL-17 well indicates a remarkably high NCG content of 21%wt and a lower temperature than other wells at the same elevation in Sikidang, suggesting its location at the system's periphery.

Heat sources in the Dieng geothermal field are discerned through high resistivity values forming doming patterns and high-temperature data. Consequently, the heat source for the Dieng geothermal field is pinpointed beneath the Pagerkandang Crater, Merdada Crater, and Pangonan Crater, which also aligns with the upflow area. In the Sileri area, the upflow is proximate to the bottom of wells WELL-10 and WELL-1 (Pagerkandang Crater) and WELL-4 and WELL-9 (Merdada Crater). Fluid flow in the Sileri area originates from the Bitingan manifestation, well pad 30 – Siglagah manifestation, and westward flow. Conversely, fluid flow in the Sikidang area emanates from the upflow around the Pangonan Crater toward the Pakuwaja Crater area and the Pulosari manifestation. Structures evolving within the Dieng geothermal field are oriented in the W-E direction, aligning with the anticline axis. This NW-SE orientation coincides with the development of volcanism, which extends NE-SW and N-S. Various factors influencing permeability, including structural features, Andesite Complex units, and damage zones associated with volcanic necks, have been identified. Several faults have been confirmed through feed zone data, encompassing Total Loss Circ7ulation (TLC), Partial Loss Circulation (PLC), and spinner data. Further investigation will be conducted to enhance understanding regarding the role of the Andesite Complex unit and volcanic neck damage zones in permeability control.

2.1.6 Material Input

In reservoir numerical modeling, boundary conditions are typically established for three key aspects: the top, side, and bottom boundaries. Petrasim® configures the conditions for the top and bottom layers using the extra cell feature. The atmospheric layer at the top of the model is used as the top boundary, where all blocks within that layer assume uniform properties. Initial conditions for temperature and

pressure are set at 20°C and 1 bar, respectively. In this layer, block values are maintained under fixed state conditions to remain unaffected by reservoir conditions throughout simulations until they attain a steady state. The model's side boundary is configured to prevent incoming or outgoing flow by assigning material properties characterized by very low permeability (1E-17 m^2) for both matrix and fracture components. The basement layer of the model serves as the bottom boundary, with extra cells incorporated to maintain constant temperature and pressure conditions while facilitating conductive heat transfer. Two sets of extra cell conditions are within the basement reservoir, namely in the Sileri and Sikidang areas. This approach aims to ensure that distinct temperature and pressure conditions can be attained for each reservoir compartment. Extra cells in the Sileri area span the entire basement reservoir. Conversely, in the Sikidang area, additional cells are exclusively implemented in the upflow section to establish conditions conducive to a flow pattern directed toward the outflow/peripheral reservoir (Figure 8).

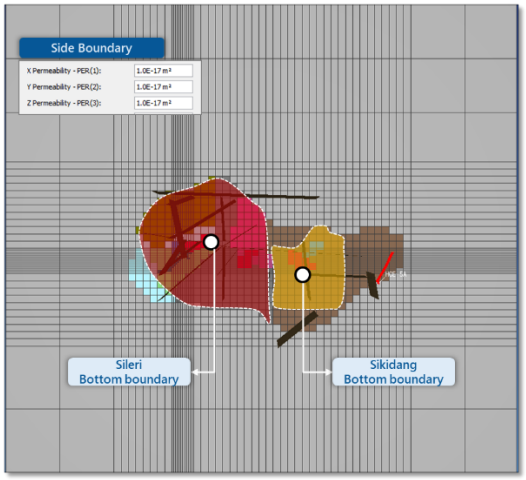

Figure 8: Boundary condition by assigning extra cells at the bottom of the model

According to the conceptual model of the Dieng geothermal field, three upflow areas have been identified: two upflows in the Sileri area and one upflow in the Sikidang area. In line with this delineation, a heat source has been modeled as a deep hot injection within these three areas. High temperatures with an enthalpy of 1,650 kJ/kg for the Sileri upflow and 1,600 kJ/kg for the Merdada upflow. A total mass rate of 46.1 kg/s is set in the Sileri area, while in the Sikidang area, hot injection is placed with an enthalpy of 1,700 kJ/kg and a mass rate of 3.7 kg/s (Figure 9a). The higher enthalpy value in the Sikidang area is intended to accommodate the presence of a steam cap within the reservoir.

In order to maintain mass balance within the reservoir, mass-out conditions are approximated by utilizing surface manifestations as discharge points. The presence of these manifestations is modeled by employing artificial wells using the well on deliverability method at constant well pressure, as illustrated in Figure 9b. This approach aims to achieve mass balance under natural reservoir conditions, wherein the mass injected into the heat source must equate to the mass discharged from the manifestations. The model incorporates six manifestations in the Sileri area and four in the Sikidang area. In the Sileri area, the manifestations include Bitingan, Sipandu, Siglagah, Kepakisan, Sileri, and Pagerkandang. Meanwhile, the Sikidang area manifestations comprise Pengilon, Sibanteng, Sikidang, and Pakuwaja. All artificial well openings representing these manifestations are in the Top of Reservoir (TOR) area.

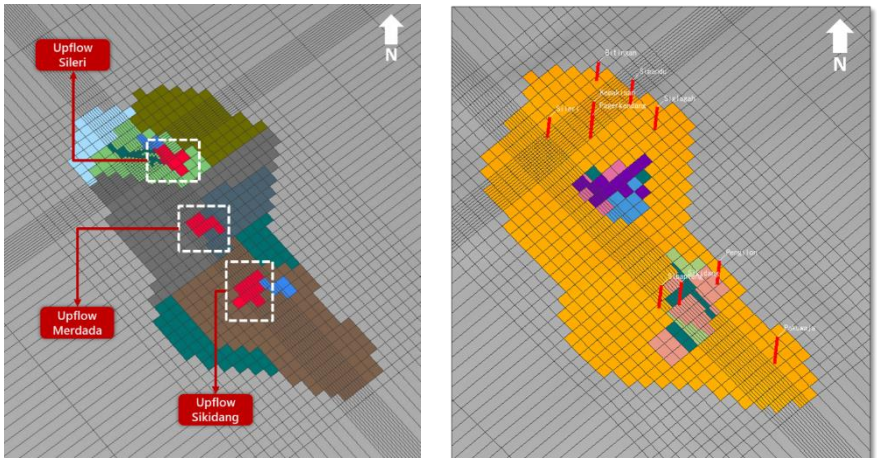

(a) (b)

Figure 9: Location of (a) deep hot injection/recharge; (b) manifestation/discharge

2.1.6 Material Properties

A dual porosity approach is employed in the natural state validation process, wherein fracture permeability emerges as the rock property exerts the most significant influence on model fluctuations. This parameter serves as the primary component in adjusting the pressure and temperature of the model. While other parameters like rock porosity may not significantly influence the natural state stage, it becomes pertinent during production history matching to align the production transients. Figure 10 illustrates the simulated distribution of fracture permeability, which aligns with the temperature and pressure data obtained from wells within the Dieng geothermal field.

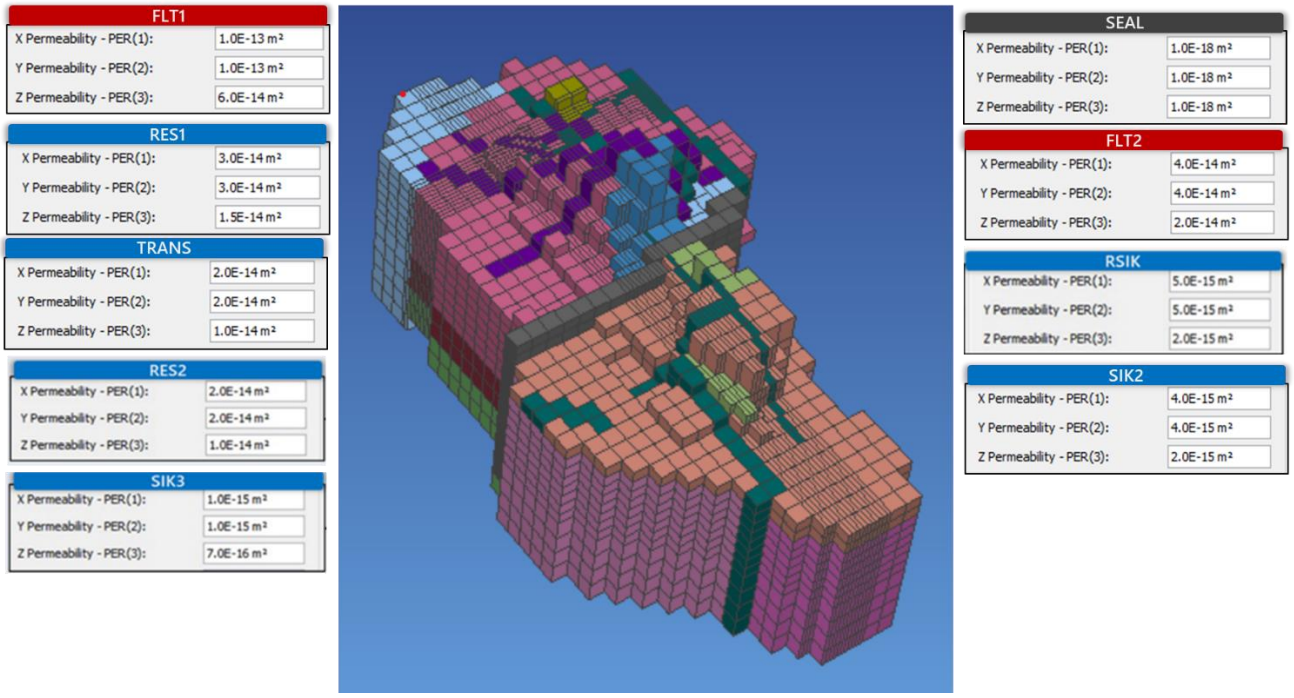

Figure 10: Fracture permeability distribution assigned in the model

The permeability distribution is assumed to be horizontally isotropic, meaning the permeability value in the lateral direction (x and y) remains the same. However, the permeability value in the vertical direction (z) is smaller. Within permeable faults, the permeability distribution ranges from 30-100 mD. The fault acting as a barrier between the Sileri and Sikidang areas (Merdada 1) is assigned a very low permeability value (0.001 mD) to impede mass transfer. However, this fault must be fully sealed from the TOR to the basement reservoir (-1750 masl). The results of the model iteration indicate that the sealing of the Merdada 1 fault is only from TOR to an elevation of -1,350 masl. This can be seen from the indication of matching pressure conditions in Sileri and Sikidang, whereby sealing to that depth, pressure balance between the two compartments can be achieved. In general, the distribution of reservoir rock permeability in the Sileri area (20-30 mD) surpasses that of the Sikidang area (1-5 mD). Consequently, the Sileri area is expected to exhibit a relatively higher well production capacity and lesser production and pressure declines compared to the Sikidang area. However, the decline in production will be influenced by the extraction rate in both reservoirs. Additionally, reservoir rock permeability distribution variations will impact reserves in each compartment. The cumulative ratio of fluid to rock in the Sileri area is anticipated to be significantly higher than in the Sikidang area. Other parameters set in the model are matrix porosity of 5% and matrix permeability of 0.01 mD. The relative permeability of rocks in the model uses Grant's curve and linear capillary pressure approach. Rock density, thermal conductivity, and rock-specific heat are set uniformly for all materials, i.e., 2,600 kg/m3, 2 W/(m.K), and 1,000 J/(kg.K).

2.2 PT Matching

Reservoir numerical simulations are carried out until the model reaches the natural state, a condition where the pressure and temperature are in a steady state that does not change or is relatively constant over time. Typically, simulations extend for 100,000 years to attain these conditions. Calibration at the natural state stage marks the initial phase of validation. This process aims to construct a model that describes temperature and pressure distribution, heat flow, mass flow, and fluid conditions in the reservoir pre-production. Additionally, it aids in identifying permeable structures and potential intrusions/heat sources within the geothermal system. Achieving a robust match between simulation results and actual data involves adjustments to fracture permeability and the mass rate and enthalpy of the heat source. The natural state calibration of the Dieng geothermal field involved a data-matching approach. This quantitative method assesses temperature and pressure deviations and the consistency of temperature patterns across different depths for each well. These evaluations aim to identify temperature pattern variations that tend to increase or decrease with depth.

2.2.1 Sileri Area

The assessment of temperature and pressure models in the Sileri is conducted separately for each wellpad. Nine wellpads were evaluated, including wellpads 7, 9, 10, 28, 29, 30, 31, 32, and 33. The WELL-1 and WELL-2 wells are directional wells directed towards the center of the Sileri reservoir, whereas the WELL-3 well is relatively vertical and positioned closer to the reservoir's peripheral area. Figure 11 illustrates PT matching for the WELL-1, WELL-2, and WELL-3 wells, all of which have reached the natural state. Among these wells, the WELL-1 well records the highest bottom hole temperature at 325°C, attributable to its proximity to the Sileri upflow area. Overall, these wells' temperature and pressure models align well with the actual temperature and pressure data conditions.

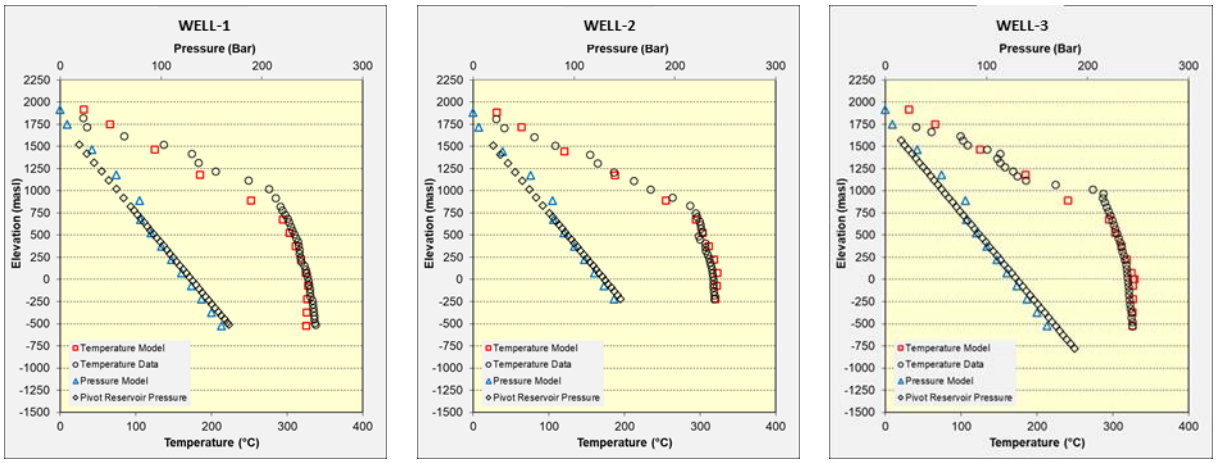

(a) (b) (c)

Figure 11: PT matching result (a) WELL-1; (b) WELL-2; (c) WELL-3

The WELL-4 and WELL-5 wells are directional wells aimed towards the center of the Sileri reservoir, while the WELL-H well is a vertical well. Figure 12 is the result of PT matching for the WELL-4, WELL-5, and WELL-H wells, which have reached the natural state. Notably, the WELL-4 well exhibits the highest temperature in this wellpad area, attributed to its location within the Merdada upflow area. These three wells' temperature and pressure models mirror the actual temperature and pressure data conditions.

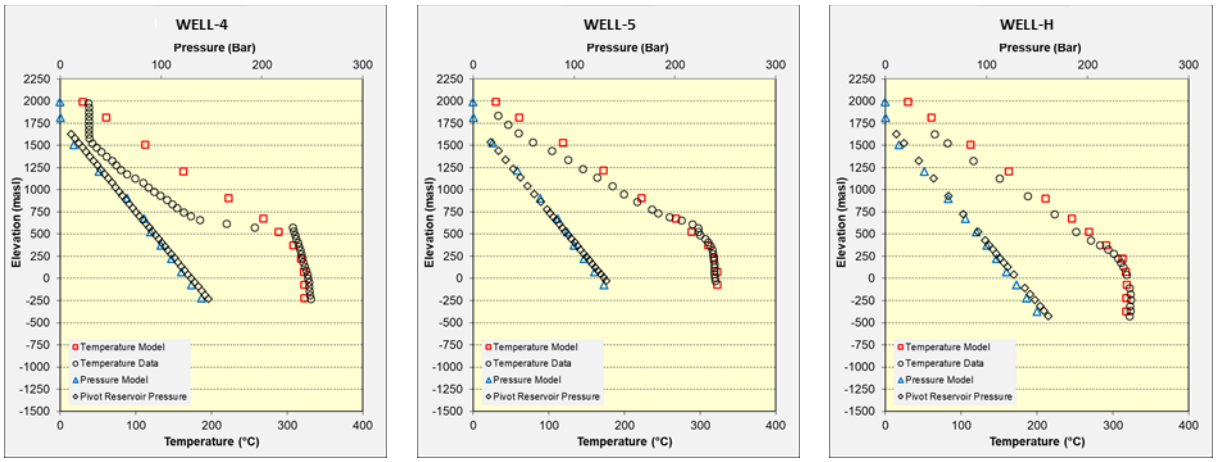

(a) (b) (c)

Figure 12: PT matching result (a) WELL-4; (b) WELL-5; (c) WELL-H

The WELL-6 well is a directional well targeting Kawan Pagerkandang, while the WELL-I well is a vertical well situated in the reservoir boundary. Figure 13 presents the PT matching results for the WELL-6 and WELL-I wells, which have reached the natural state. The PT matching reveals that the model temperature and pressure of the WELL-I align with the actual data. However, the model temperature of the WELL-6 well still appears to be higher than the actual data. The exact temperature conditions of the WELL-6 well were evaluated by examining the data post the operationalization of Dieng Unit 1. Despite the WELL-6 well never being online since well-testing activities in 1997, comparing the 2020 logging data remains relevant enough to serve as a reference for model validation for this well.

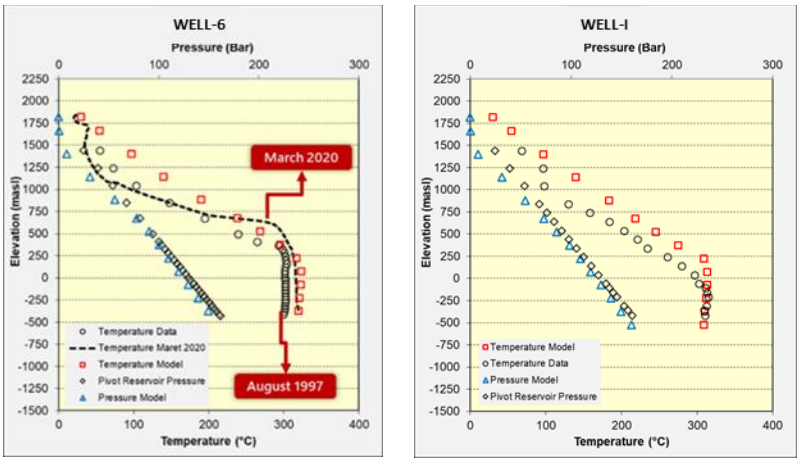

(a) (b)

Figure 13: PT matching result (a) WELL-6; (b) WELL-I

Wellpad 28 is located at the center of the Sileri reservoir area, with two wells targeted towards its core: WELL-8 and WELL-9. WELL-7, a directional well, is aimed towards the peripheral reservoir and is situated near the boundary of the Sikidang reservoir. Figure 14 presents the PT matching results for the WELL-7, WELL-8, and WELL-9, which have attained the natural state. The temperature and pressure of the WELL-7 well model exhibit perfect agreement with the actual data. However, the temperature models for the WELL-8 and WELL-9 wells show relatively higher temperatures compared to the actual data (8 – 10°C in the liner area). In the case of the WELL-8 well, the quality of the actual data tends to be insufficient, resulting in the model temperature data being poorly adjusted to actual conditions. This discrepancy is evidenced by the temperature data, which tends to decrease with increasing depth, an anomaly not observed when the well is directed toward the upflow.

WELL-10 and WELL-11 represent the wells with the highest bottom hole temperature among all the wells in the Dieng geothermal field, reaching 339°C. These elevated temperature conditions result from the precise directional positioning of the wells within the Sileri upflow area, particularly for WELL-10. Figure 15 displays the PT matching results for WELL-10 and WELL-11. The graphical representation of the actual data illustrates a close alignment between the temperature and pressure of the two wells. Furthermore, model temperature and pressure deviation appear relatively minimal compared to the actual data.

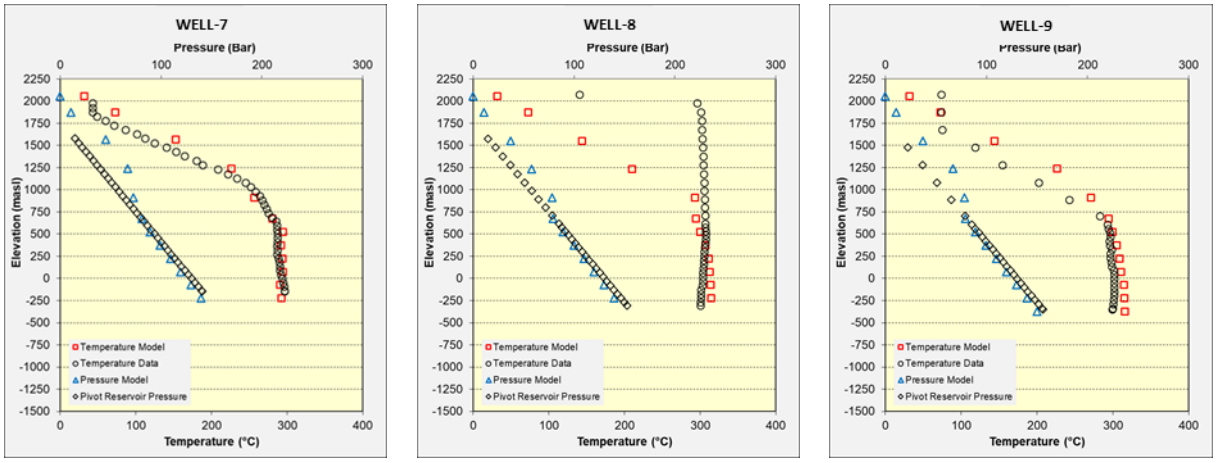

(a) (b) (c)

Figure 14: PT matching result (a) WELL-7; (b) WELL-8; (c) WELL-9

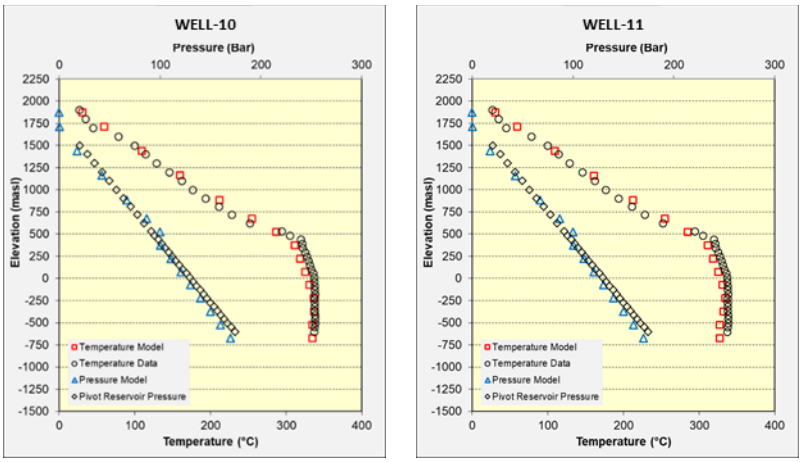

(a) (b)

Figure 15: PT matching result (a) WELL-10; (b) WELL-11

Similar to the majority wells in the Sileri area, the two wells in Wellpad 30 are primarily aimed at accessing the reservoir. Located between the Sileri and Merdada upflow zones, WELL-12 and WELL-13 represent this targeting strategy. Figure 16 displays the PT matching results for both wells. The model temperature profiles for WELL-12 and WELL-13 closely align with actual conditions from the surface to the bottom hole. Notably, the pressure profile indicates a boiling zone in the TOR section, reflecting the distribution of the steam cap within the Sileri reservoir.

Figure 17a presents the PT matching results for WELL-14. Comparison between the model and actual temperature and pressure profiles reveals a significant distribution of the boiling zone within this well. This distribution is attributed to the shallow TOR condition, establishing it as a fluid conduit zone within the reservoir. Additionally, WELL-14 exhibits relatively high productivity due to its intersection with the Pangonan fault, characterized by a permeability of 100 mD. Overall, the temperature distribution depicted in the model closely corresponds to the actual temperature data.

Figure 17b depicts the PT matching outcomes for WELL-15. Despite its location in the Sikidang area, WELL-15 is classified as a Sileri area well due to its traversal through the sealing fault (Merdada 1) and penetration into the Sileri area. The temperature and pressure profiles of the model closely align with the actual conditions of the well. At an elevation of 500 masl, the model's pressure profile appears slightly lower than the reservoir pressure distribution. This discrepancy arises as the WELL-15 well intersects the Merdada 1 fault at this depth, acting as a sealing structure separating the Sileri and Sikidang reservoir areas.

The PT matching results for WELL-16 are illustrated in Figure 17c. Similar to WELL-6, WELL-16 is a well situated within the Pagerkandang Crater. Additionally, it remains idle while Unit 1 is operational. The modeled and actual pressure profiles exhibit relatively good alignment. However, the model temperature profile reflects higher conditions than the actual well temperature. To address this, the exact temperature conditions of WELL-16 were scrutinized by referencing data post-operations of Dieng Unit 1. The addition of PT shut-in logging data in 2020 provided further validation for the WELL-16 well model. In the 2016 data, despite the MCD only reaching an elevation of 500 masl, it's evident that the maximum temperature at that depth surpasses the actual data from 1998. Similarly, with the temperature conditions logged in 2022, the model temperature tends to align more closely with 2016 and 2022 data. This suggests that the 1998 temperature data has not stabilized under equilibrium conditions.

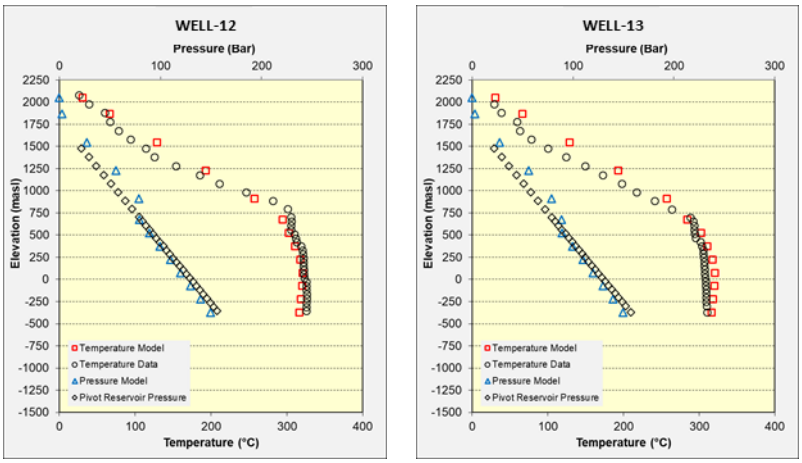

(a) (b)

Figure 16: PT matching result (a) WELL-12; (b) WELL-13

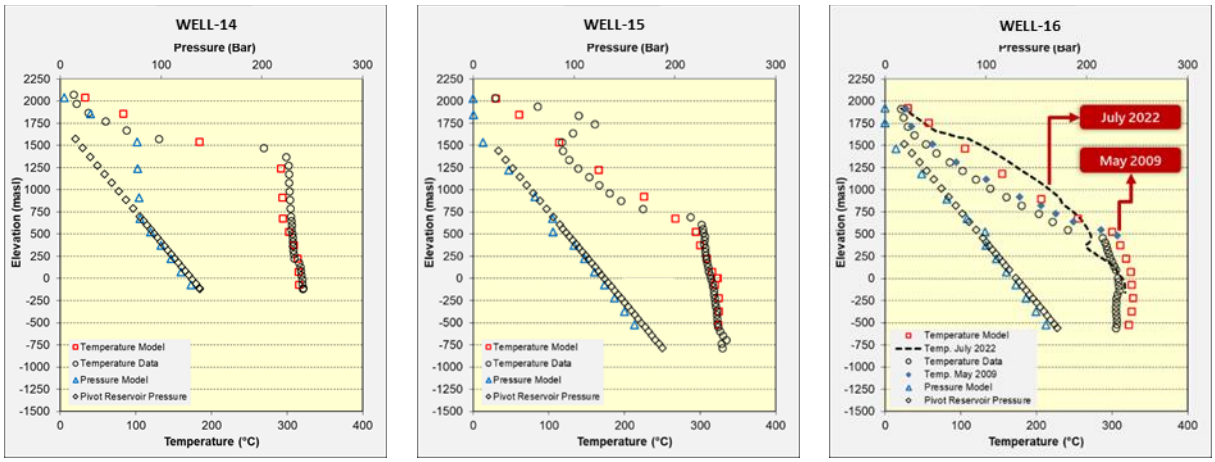

(a) (b) (c)

Figure 17: PT matching result (a) WELL-14; (b) WELL-15; (c) WELL-16

2.2.2 Sikidang Area

Evaluation of temperature and pressure models in the Sikidang area is segmented by each wellpad. Six wellpads were assessed, i.e., wellpads 24, 3, 26, 17, 18, and 20. Figure 18 shows the PT matching results of WELL-F and WELL-O. The temperature and pressure profiles of the WELL-O model align with the actual data conditions. However, in the WELL-O well, the model temperature tends to be lower than the actual temperature. Adjusting the exact temperature of the WELL-O well in the model is challenging due to its high-temperature distribution, reaching up to 332°C. Adjustments in this area may impact the temperature distribution across the model, potentially causing discrepancies in other wells. Nevertheless, this condition is deemed acceptable since the convective temperature pattern remains consistent with the actual data. The PT matching results of WELL-C and WELL-Y are presented in Figure 19. Overall, the model's temperature and pressure profiles for both wells closely match the actual data. WELL-C is situated at the reservoir boundary, as evidenced by its bottom hole temperature reaching only 268°C, indicating its proximity to the outflow zone of the geothermal system in the Sikidang area. Additionally, the temperature profile of WELL-C exhibits a reversal pattern. Conversely, WELL-Y boasts one of the highest bottom hole temperatures in the Sikidang area, at 324°C. This is because the WELL-Y is located in the Sikidang upflow zone, which is characterized by significant magmatic activity in the Dieng geothermal field.

Figure 20a illustrates the PT matching outcomes for WELL-P. Positioned as a vertical well within the peripheral boundaries of the Sikidang reservoir, WELL-P exhibits model temperature and pressure profiles that closely align with the actual data. Figure 20b and Figure 20b presents the PT matching results for WELL-Q and WELL-S, both vertical wells situated differently within the Sikidang reservoir. WELL-Q, located in the northern peripheral zone, exhibits model temperature and pressure profiles closely resembling the actual data. The convective pattern extends continuously to the bottom hole across the model and actual data. Conversely, WELL-S, positioned between the upflow and outflow zones, shows a reversal pattern in both the model and actual data. The sharper pattern observed in the actual data's bottom hole area might be attributed to localized permeability, preventing the drilling fluid's temperature from reaching equilibrium during the well heating-up phase.

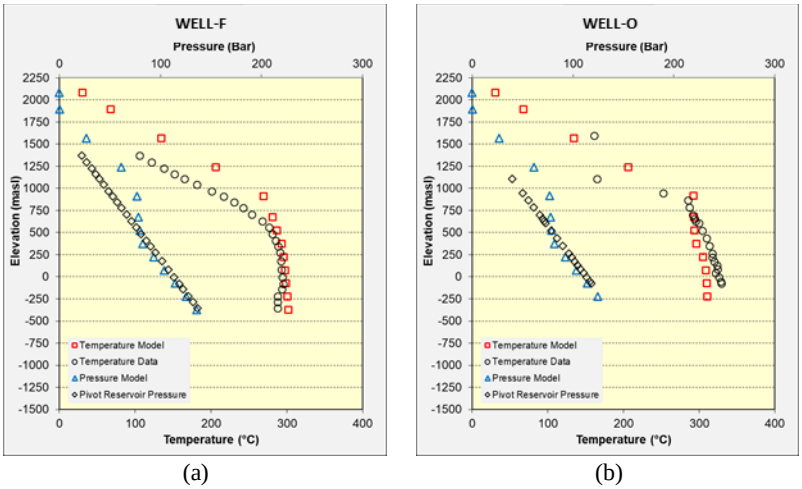

(a) (b)

Figure 18: PT matching result (a) WELL-F; (b) WELL-O

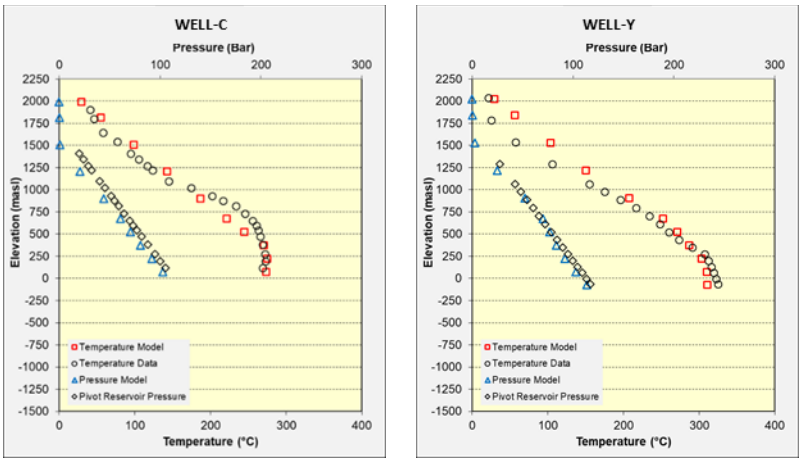

(a) (b)

Figure 19: PT matching result (a) WELL-C; (b) WELL-Y

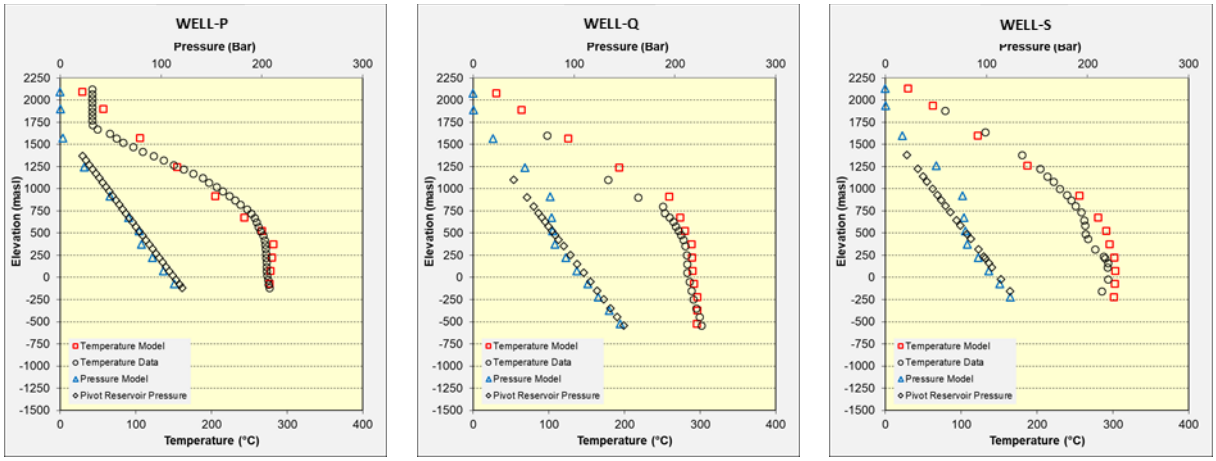

(a) (b) (c)

Figure 20: PT matching result (a) WELL-P; (b) WELL-Q; (c) WELL-S

2.3 Temperature, Preussre, and Steam Saturation Distribution

Figure 21 shows a cross-section of the natural state temperature distribution in the Dieng geothermal field. The temperature distribution shows three upflows: Sileri, Merdada, and Sikidang. The Sileri area exhibits the highest upflow temperatures, followed by Merdada and Sikidang. The updoming pattern is visible in the Merdada upflow zone. This is in accordance with the conditions of the wells in this area, i.e., WELL-14 and WELL-8, which have a relatively thick boiling zone. The Sikidang area reservoir shows hot support associated with the Sikidang upflow zone, with the direction of heat flow towards the southern outflow (WELL-17), which is related to the presence of the Pakuwaja manifestation. The pressure contrast between the Sileri and Sikidang areas, as illustrated in Figure 22, delineates the reservoir compartments for each zone. Broadly, the Sileri region exhibits higher pressure levels compared to the Sikidang area. This alignment coincides with the pressure assessments conducted based on the pivot evaluation. Under lower pressure conditions, the steam cap distribution in the Sikidang area is more extensive, characterized by higher saturation levels compared to the Sileri area, as depicted in Figure 23.

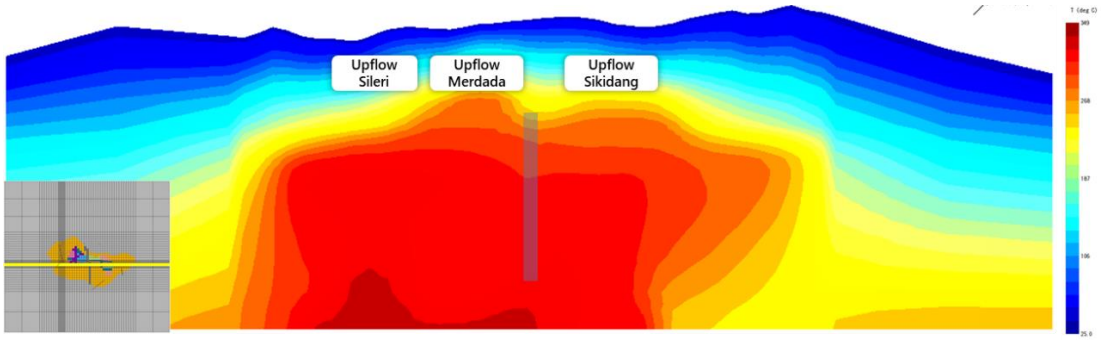

Figure 21: Cross-section of the natural state temperature distribution

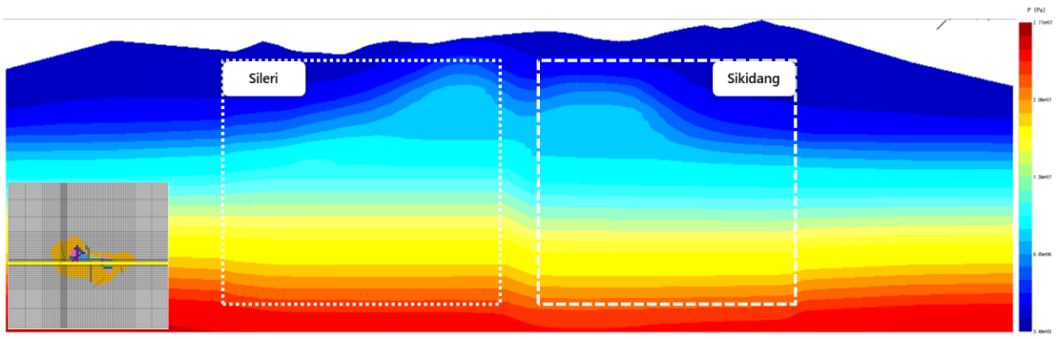

Figure 22: Cross-section of the natural state pressure distribution

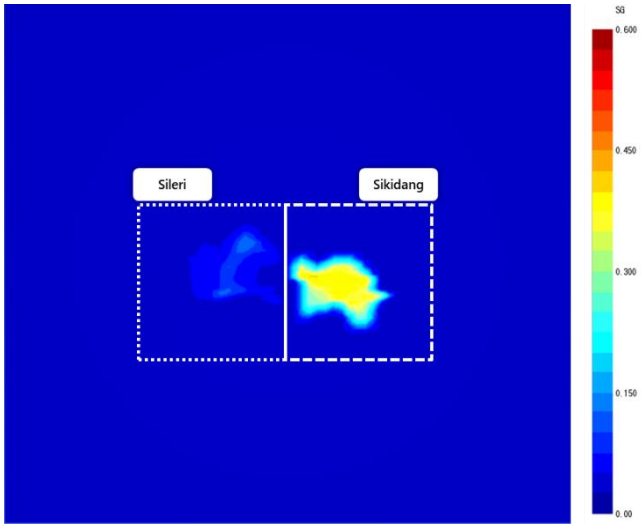

Figure 23: Cross-section of the natural state steam saturation

3. HISTORY MATCHING

Once satisfactory matching results have been achieved between the temperature and pressure values derived from the simulation outcomes and the actual data, the subsequent phase involves production history matching. This calibration process aims to synchronize the model's natural state outcomes with the production and injection dynamics of Unit 1, which has been operational for 20 years since its Commissioning Date (COD) in 2002.

3.1 QA/QC Production and Injection Data

QA/QC results for each production and injection data are shown in Figure 24 and Figure 25.

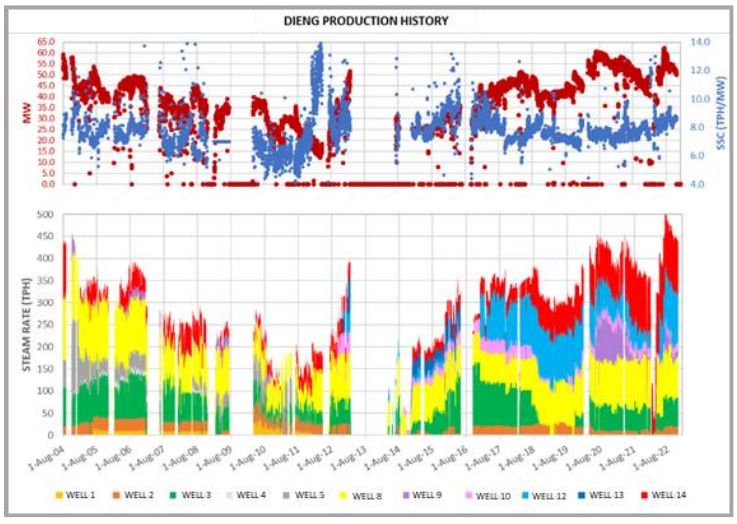

Figure 24: QA/QC results of production data

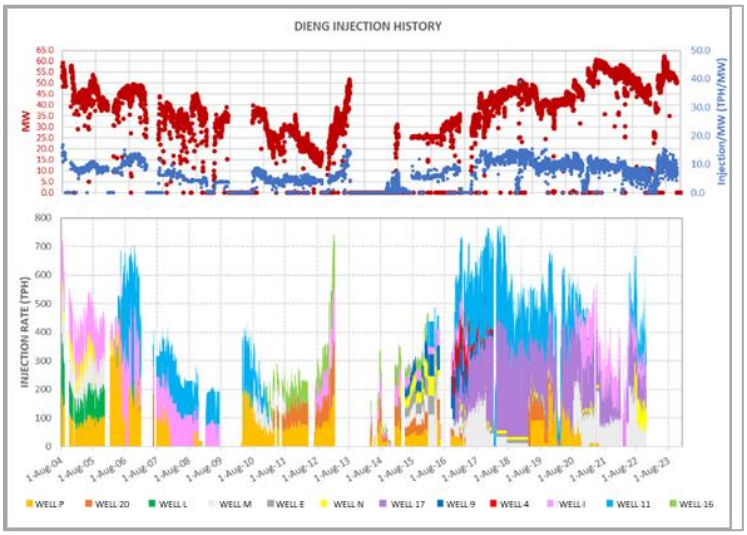

Figure 25: QA/QC results of injection data

3.2 Model Calibration

In production history matching, two primary approaches are commonly used: mass out and well-on deliverability.

1. Mass Out Approach: This method involves determining the total mass extracted from the reservoir, which can vary either constantly or over time. This approach calculates and inputs the total mass produced and injected into the model. This is particularly useful when there are fluctuations in mass amounts during production and injection periods.
2. Well-on Deliverability Approach: This method focuses on determining the Productivity Index (PI) value and the bottom hole pressure of the well. It provides insights into the efficiency of the well and its ability to produce fluids from the reservoir.

In this model, the mass-out approach is employed due to the fluctuations in mass amounts over time during production and injection periods. Additionally, when the feed zone is incorporated into the model, the quantity of feed zone openings may exceed one grid block due to the relatively small layer thickness (100 m). Consequently, production and mass injection in the reservoir are adjusted using the kh value, with production and injection ratios typically higher in grid blocks with higher permeability.

The history-matching results for WELL-1 indicate a good match between the actual and model total mass flow production distribution, as shown in Figure 26a. However, due to the absence of enthalpy measurement data based on the TFT conducted in 2012, the model's enthalpy values cannot be validated against actual data. Without TFT data, the model's enthalpy values remain relatively constant from 2004 to 2022, averaging around 1,470 kJ/kg to 1,480 kJ/kg. While this provides a consistent profile within the model, the lack of validation against actual enthalpy measurements from TFTs leaves some uncertainty regarding the accuracy of the model's enthalpy representation for WELL-1 during that period.

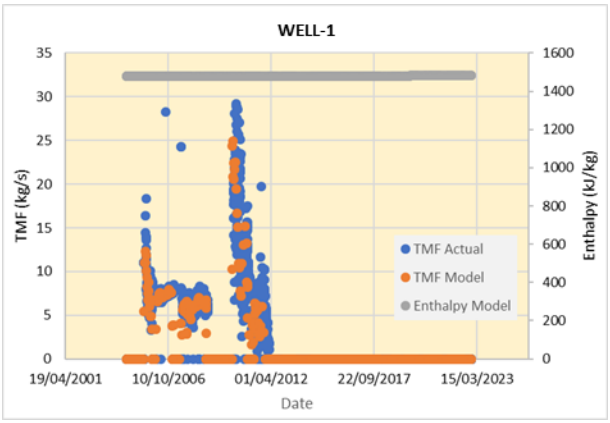

(a)

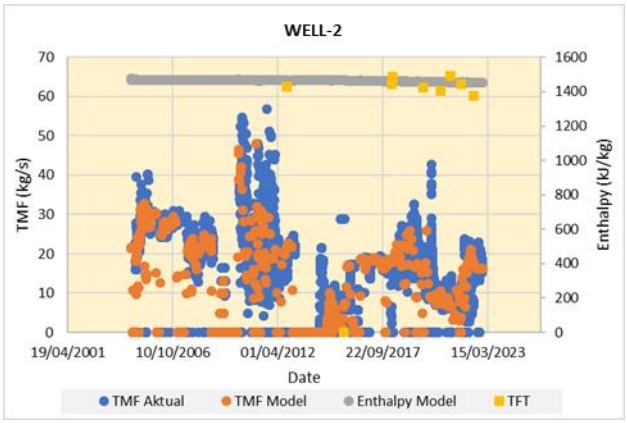

(b)

Figure 26: Production history matching result of (a) WELL-1; (b) WELL-2

The history-matching results for WELL-2 indicate a good match between the actual and model total mass flow production distributions, as illustrated in Figure 26b. This well intersects two grid block layers at elevations of 225 masl and 75 masl, corresponding to fault materials with high permeability (100 mD). TFT data for WELL-2, obtained in 2012, 2015, 2018, 2019, 2020, 2021, and 2022, provides valuable insights into the well's enthalpy behavior. Despite fluctuations, the TFT data indicates a relatively constant enthalpy value over

time. The enthalpy of the WELL-2 well model during production was 1,475 kJ/kg, decreasing slightly to 1,451 kJ/kg by 2022. The distribution of model enthalpy closely aligns with the TFT enthalpy values, demonstrating good agreement between the model's representation and the actual enthalpy behavior observed during TFT.

The history-matching results for WELL-3 demonstrate a good match between the actual and model total mass flow production distributions, as depicted in Figure 27a. This indicates that the model effectively captures the production behavior observed in the field. Five instances of TFT data are available for WELL-3, covering 2018, 2020, 2021, and 2022. The TFT enthalpy values for this well exhibit relative stability, ranging from approximately 1,454 kJ/kg to 1,525 kJ/kg, with a notable spike observed in 2018 around 1,634 kJ/kg. During the production period, the enthalpy of the WELL-3 well model remained relatively stable, fluctuating between 1,504 kJ/kg and 1,494 kJ/kg. The distribution of model enthalpy compared to TFT enthalpy shows reasonably good qualitative agreement, indicating that the model accurately represents the enthalpy behavior observed during TFT.

For WELL-4, which lacks TFT data, the model's enthalpy cannot be directly validated against actual enthalpy. The model's enthalpy value remains relatively stable throughout the period, hovering around 1,480 kJ/kg. Regarding WELL-5, it was in production from 2004 to 2011. The history-matching results reveal a good alignment between the actual and model total mass flow production distributions, as illustrated in Figure 28a. However, since the first TFT in the Dieng geothermal field occurred in 2012 after WELL-5 ceased production, the model's enthalpy cannot be verified against actual enthalpy. The model's enthalpy values remain relatively consistent from 2004 to 2022, ranging from approximately 1,457 kJ/kg to 1,471 kJ/kg.

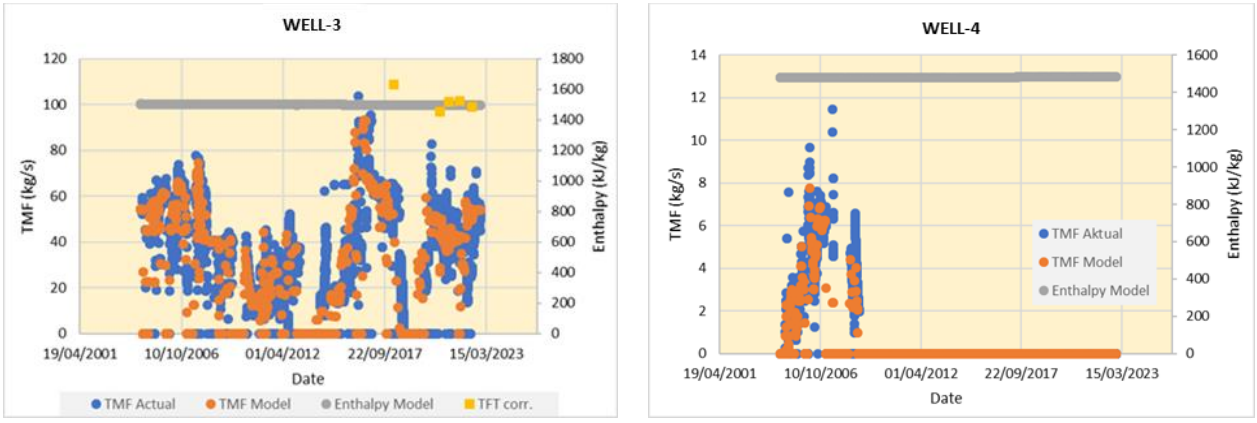

(a) (b)

Figure 27: Production history matching result of (a) WELL-3; (b) WELL-4

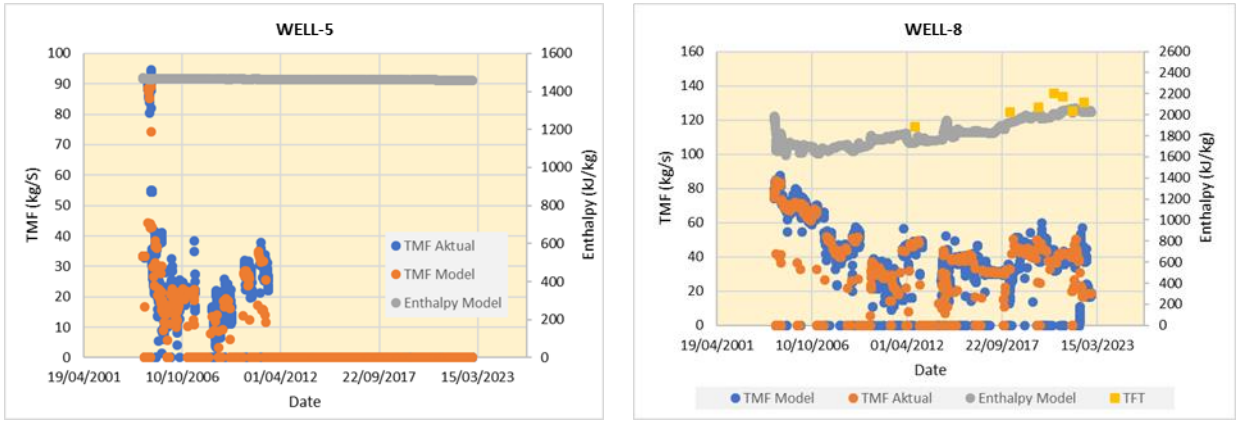

(a) (b)

Figure 28: Production history matching result of (a) WELL-5; (b) WELL-8

The production data for WELL-8 suggests that the well experiences constant cyclic WHP (Well Head Pressure) variations. During these cycles, WHP tends to increase, leading to increased brine production due to decreased dryness. This phenomenon is attributed to the support feed zone area, where brine can contribute due to minimal bottom-hole pressure differences over a short period. Reservoir simulation can approximate these conditions when cyclicity occurs, as the feed zone opened in the model exists within the steam and brine area. The history-matching results demonstrate a good alignment between the actual and model total mass flow production distributions (Figure 28b). The model effectively captures the actual enthalpy changes from 2012 to 2022. The evolution of the model's enthalpy linearly increases from 1,600 kJ/kg to around 2,100 kJ/kg during this period. This trend suggests a tendency for higher steam saturation in the reservoir due to ongoing production activities.

WELL-9 has three good-quality TFT data points recorded for 2020, 2021, and 2022. Across these periods, the TFT enthalpy value remains relatively constant, ranging from 1,358 kJ/kg to 1,423 kJ/kg. During the production period, the enthalpy of the WELL-9 well model remains stable, varying between 1,379 kJ/kg and 1,383 kJ/kg (Figure 29a). The qualitative comparison between the model and TFT enthalpy indicates reasonably good agreement. The TFT data for WELL-10 with good data quality are 2012, 2015, 2018, 2019, 2020, 2021, and 2022. The TFT data indicates a relatively constant enthalpy value with some fluctuations throughout these periods. During the production period, the enthalpy of the WELL-10 well model remained fairly stable, ranging from 1,520 kJ/kg to 1,616 kJ/kg. Qualitatively, the distribution of model enthalpy to TFT enthalpy shows reasonably good agreement (Figure 29b).

The history matching results for WELL-12 indicate a good match between the actual and model total mass flow production distributions (Figure 30a). However, there is a significant deviation in the enthalpy values, with the model enthalpy being higher than the actual enthalpy. The QC results of TFT enthalpy data for 2018, 2019, 2020, 2021, and 2022 indicate good data quality. Brine geochemical data suggests no meteoric water intrusion into the well, which could result in cooling. The hypothesis for the low actual production enthalpy is the presence of condensate in the steam cap section, resulting in dilution into the well. This hypothesis is supported by a decrease in cations, especially Na, without any anomaly in Mg concentration, suggesting a dilution process with non-reservoir fluid, likely condensate. Unfortunately, this dilution approach cannot be incorporated into the reservoir numerical simulation model. Therefore, the model enthalpy condition reflects the actual enthalpy of the WELL-12 well without any dilution, ranging from around 1,447 kJ/kg to 1,460 kJ/kg. As for the WELL-13 well, since no TFT data is available, validation of the model enthalpy against the actual enthalpy cannot be carried out. The model enthalpy value for WELL-13 indicates a relatively constant profile, around 1,427 kJ/kg (Figure 30b).

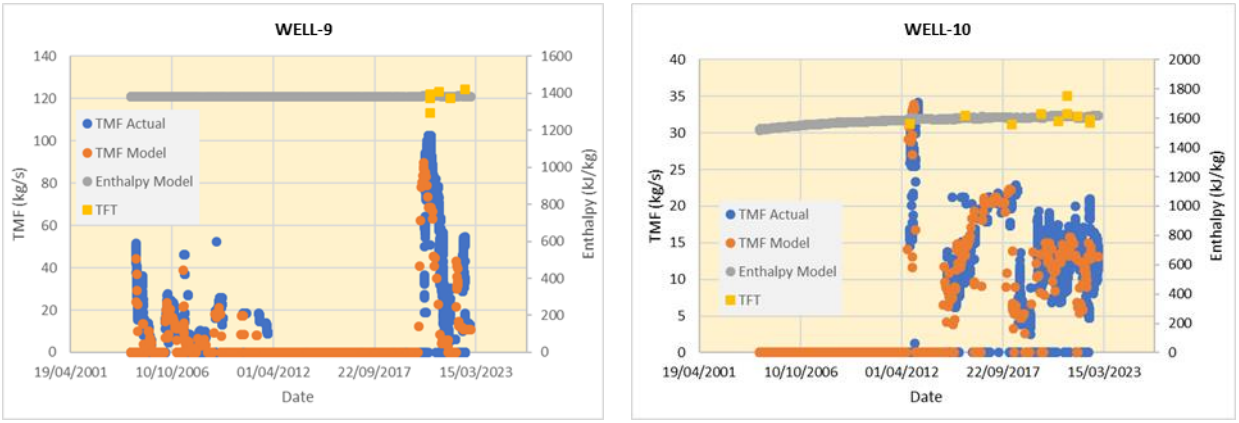

(a) (b)

Figure 29: Production history matching result of (a) WELL-9; (b) WELL-10

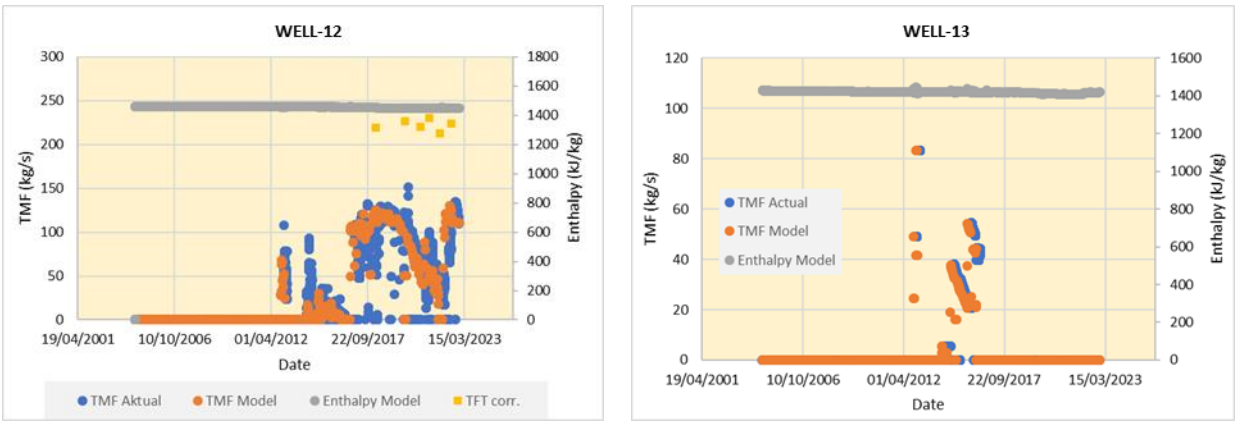

(a) (b)

Figure 30: Production history matching result of (a) WELL-12; (b) WELL-13

The WELL-14 well underwent significant enthalpy changes over time, indicating an evolution of conditions within the reservoir. During well testing in 1998, the enthalpy values were relatively low, ranging from around 1,426 kJ/kg to 1,475 kJ/kg, accompanied by considerable brine production. However, after the first TFT in 2018, the production enthalpy surged to a very high value of 2,601 kJ/kg, which remained constant in subsequent TFT measurements from 2019 to 2022, fluctuating between 2,634 kJ/kg to 2,724 kJ/kg (Figure 31a). In reservoir numerical simulation, the evolution of enthalpy in the WELL-14 well can be validated by minimizing the permeability distribution in the area. This approach reduces the mass within the reservoir, allowing phase changes due to boiling to occur more rapidly with mass extraction. Furthermore, steam tends to be more mobile at low permeability conditions than brine, influencing the enthalpy distribution. Both qualitatively and quantitatively, the distribution of model enthalpy to TFT enthalpy has shown relatively good agreement, indicating that the simulation captures the evolving conditions within the reservoir reasonably well.

Figure 31b provides a compilation of pressure drops observed during the production history matching. All wells exhibit a similar decline pattern, characterized by two distinct periods: a decline period from 2004 to 2015 and another from 2016 to 2022. The decline rate averages 0.17% per year during the first period, while it increases to 0.53% per year in the second period. This decline pattern aligns with the power generation trends, which fluctuated at less than 40 MW until 2015 before rising to more than 40 MW and reaching up to 60 MW starting in 2016. The increase in power generation likely corresponds to changes in reservoir dynamics and production strategies over time, leading to variations in pressure drop rates across the production wells.

After production and injection activities occur, changes occur in the natural state model's temperature, pressure, and steam saturation conditions. The fluctuations in these parameters depend on the amount of mass extracted and injected into the reservoir. Greater mass extraction leads to more significant pressure drops and increases in steam saturation. These changes were validated by new wells drilled for the Dieng 2 unit. Six wells were drilled at the time of writing this report: NEW-WELL-1, NEW-WELL-2, NEW-WELL-3, NEW-WELL-4, SLR-J-7D, and SLR-J-7E. However, heating-up data is only available for four wells: NEW-WELL-1, NEW-WELL-2, NEW-WELL-3, and NEW-WELL-4. It's important to note that the temperature of these four wells has not yet reached equilibrium conditions, as there are still indications of temperature reversal in the bottom hole area. The heating-up duration for each well is as follows: NEW-WELL-1 (144 days), NEW-WELL-2 (120 days), NEW-WELL-3 (123 days), and NEW-WELL-4 (82 days).

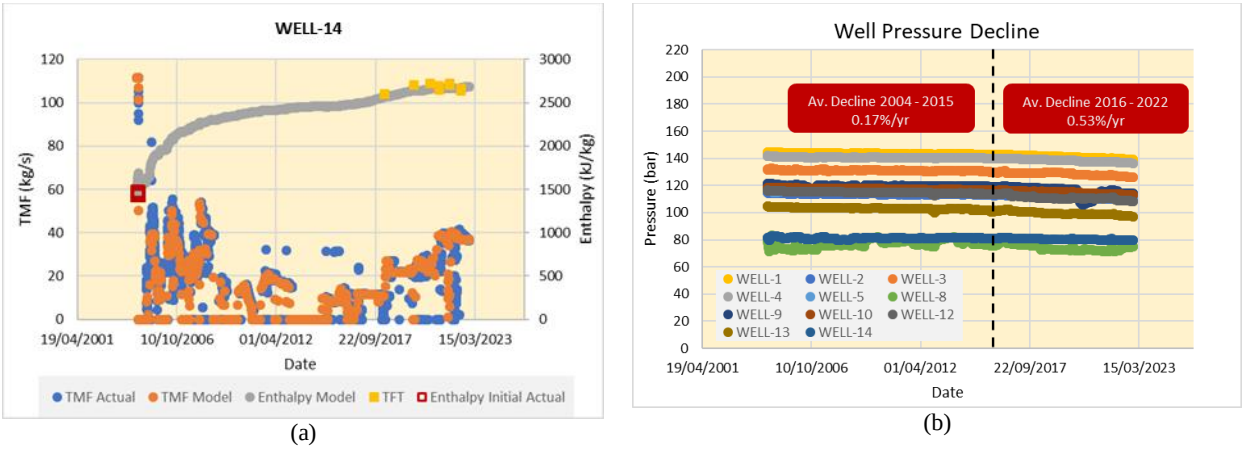

Figure 31: (a) production history matching result of WELL-14; (b) compilation of pressure decline during production

Figure 32 shows the PT matching results and model conditions following production history matching. The temperature profiles of both NEW-WELL-1 and NEW-WELL-2 wells indicated a similar trend, with the temperature in the steam area matching well due to reaching equilibrium. However, the temperature in the brine area still displays a reversal, indicating that equilibrium conditions have not yet been reached. Regarding pressure profiles, both wells show a transition zone between the water level and the steam cap zone at an elevation of 500 masl. This transition zone indicates the boundary between the liquid and vapor phases within the reservoir. Compared with the natural state based on the WELL-14 well, it is observed that the steam cap thickened by around 200 meters from 2004 to 2022. Understanding these pressure and temperature profiles is crucial for managing the reservoir effectively and optimizing production strategies. It allows operators to monitor changes in reservoir conditions over time and make informed decisions to maximize energy extraction while maintaining reservoir integrity and sustainability. Similar to NEW-WELL-1 and NEW-WELL-2, the PT matching results for NEW-WELL-3 and NEW-WELL-4 after production history matching display a similar pattern (Figure 33). The temperature profiles at the top of the reservoir area exhibit actual temperatures that have reached equilibrium conditions, aligning well with the model temperatures. However, a reversal in actual temperatures is observed in the bottom hole area.

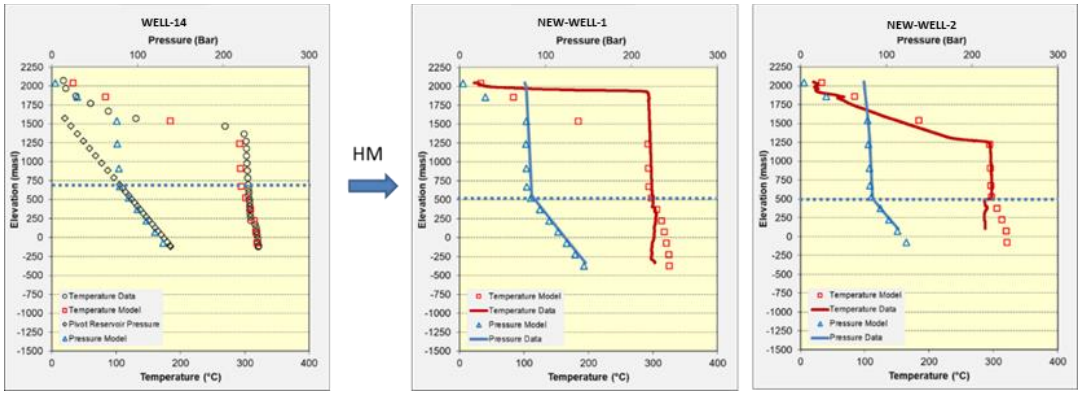

Figure 32: PT matching of NEW-WELL-1 and NEW-WELL-2 wells and pressure correlation with steam cap thickening

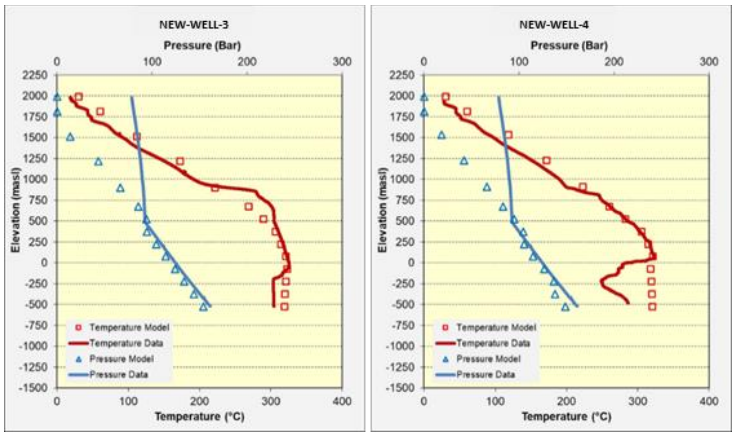

Figure 33: PT matching of new drilled wells; (a) NEW-WELL-3; (b) NEW-WELL-4

The production area of Unit 1 primarily encompasses the Sileri area, while the injection area is predominantly in the Sikidang area. In Sileri, the impact of mass extraction leads to a reduction in reservoir pressure, directly influencing the formation of steam caps in the vicinity. However, because most of the injections are directed towards the Sikidang area, temperatures in the surrounding regions tend to decrease gradually over time. Figure 34 shows the temperature variations from the natural state to after-production history matching. The most significant temperature decline is observed in WELL-17, situated in the Sikidang area. Conversely, WELL-I and WELL-11 in the Sileri area show a relatively minor decrease in temperature.

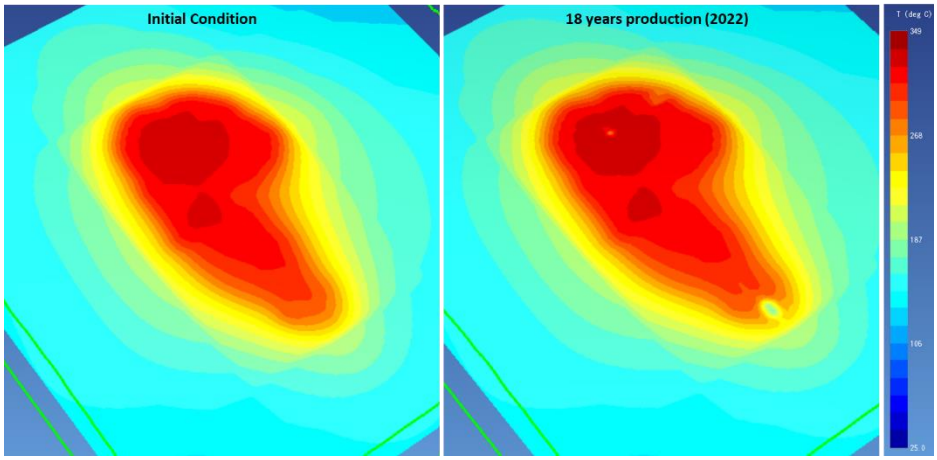

Figure 34: Reservoir temperature distribution after history matching at 0 masl

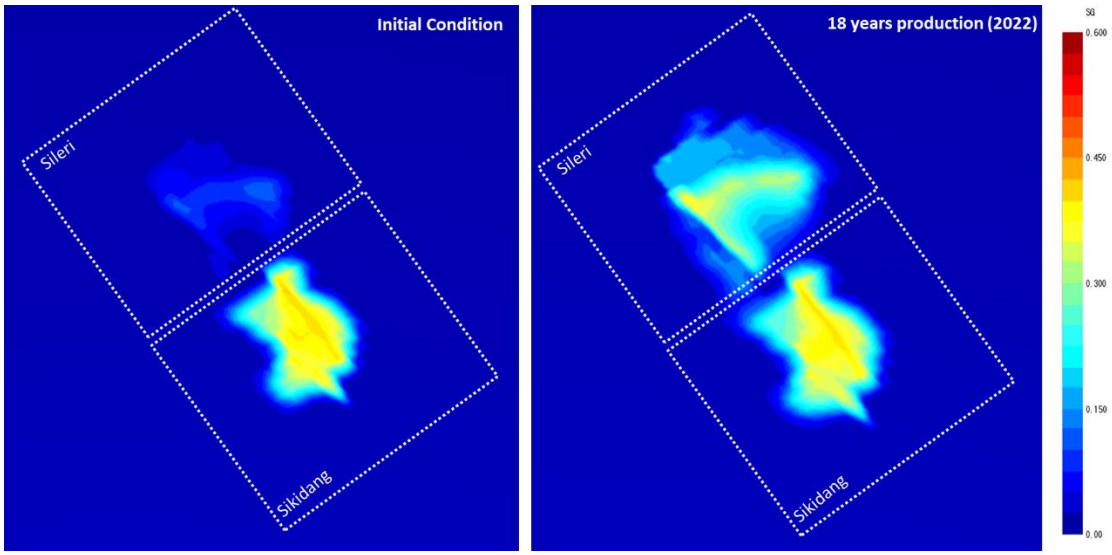

Figure 35: Steam saturation distribution after history matching at 500 masl

Figure 35 illustrates the steam saturation progression and the steam cap's development within the reservoir. Initially, the natural state analysis reveals the presence of a steam cap within the Sileri area, situated at an elevation of 500 meters above sea level, spanning wellpads 28, 31, 30, and 7. However, the steam saturation levels remain relatively modest, ranging between 10% and 15%. Following Unit 1 production and injection activities, the history matching model indicates a notable expansion of the steam cap distribution, particularly within the Sileri area. Significant horizontal expansion is observed within wellpad areas 31, 28, and 7, with steam saturation levels ranging between 20% and 40%. At the interface of the Sileri and Sikidang regions, the WELL-9 well is situated within the steam cap transition zone, characterized by a lower steam saturation of approximately 10%. These findings underscore the impact of production and injection activities on the evolution of the steam cap, emphasizing the importance of monitoring steam saturation dynamics for effective reservoir management.

4. DISCUSSION

The numerical simulation of the Dieng reservoir has undergone significant enhancements, incorporating additional data, notably from the Dieng 2 drilling results. The updated simulation yields improved accuracy with a refined grid block size, aligning well with the natural state and history-matching results across temperature, pressure, and steam saturation distribution. This comprehensive update enables a detailed depiction of the reservoir's evolution over 20 years of production, elucidating the development of the steam cap and the consequential shifts in temperature and pressure resulting from production and injection activities. The simulation offers valuable insights into the reservoir's dynamic characteristics, providing crucial information for effective reservoir management strategies.

Forecasts regarding reservoir performance have been conducted for Units 1, 2, 3, and 4, situated in the Sileri area. However, the detailed forecast outcomes will be presented in a separate publication. The model's response to the forecast results over a 30-year period suggests that the reservoir in the Sileri area remains capable of supporting all four units during this timeframe. The forecasts encompass various injection scenarios, including the use of both cold brine and hot brine, aimed at assessing reservoir sustainability. These scenarios aim to evaluate the long-term viability of the reservoir under different operational conditions and provide valuable insights into potential strategies for sustained reservoir management.

In order to enhance the accuracy of the reservoir model for the Sikidang area, it is imperative to incorporate current pressure and temperature data. This additional data is essential for validating the existing steam cap condition in the area, especially given the allocation of most of Unit 1's injection to Sikidang. By integrating this data, the reliability and confidence in the model results for the Sikidang area will be significantly improved. This, in turn, will enable more accurate forecasts to be generated to meet the 400 MW ESC target.

5. ACKNOWLEDGEMENTS

The author would like to thank the management of PT Geo Dipa Energi (Persero) for permission to publish this work.

6. REFERENCES

Ashat A., Ridwan R. H., Prabata W., Situmorang J., Elfina, Adityawan S., Ibrahim R. F. (2019) Numerical Simulation Update of Dieng Geothermal Field, Central Java, Indonesia, 41st New Zealand Geothermal Workshop, 25-27 November 2019, Auckland, New Zealand

Pratama H. B., Supijo C. S., Sutopo (2020) Experimental Design and Response Surface Method in Geothermal Energy: A Comprehensive Study in Probabilistic Resource Assessment, Geothermics, Volume 87. https://doi.org/10.1016/j.geothermics.2020.101869

Pruess, K., Narasimhan, T.N. (1985) A Practical Method for Modeling Fluid and Heat Flow in Fractured Porous Media, Society of Petroleum Engineers Journal, 25(1), 14-26.

Supijo C. S., Pratama H. B., Sutopo (2019) Leapfrog's 3D Temperature Distribution Based on TOUGH2 Numerical Modelling: A New Approach, 41st New Zealand Geothermal Workshop, 25-27 November 2019, Auckland, New Zealand

Warren JE, Root PJ. (1963) The behavior of naturally fractured reservoirs. SPEJ. 1963;3(03):245–55. https ://doi.org/10.2118/426-PA.